Reflection limitation by driven stimulated Brillouin rescattering and finite-bandwidth spectral interaction

Carlos Montes
Groupement de Recherches Coordonnées (GRECO) Interaction Laser-Matière, Laboratoire de Physique de la Matière Condensée, Parc Valrose, F-06034 Nice Cédex, France*
and Observatoire de Nice, Boîte Postale 139, F-06003 Nice Cédex, France
(Received 17 September 1984)

Driven stimulated Brillouin rescattering, obtained by a multiline laser light, each satellite line downshifted by twice the acoustic frequency, is an efficient way to reduce stimulated Brillouin reflection [C. Montes, Phys. Rev. Lett. **50**, 1129 (1983)]. An explicit reflection formula for two input lines depleting in a finite, homogeneous plasma slab—in the heavy ion-damping limit—is obtained which generalizes Tang's formula for one single input line. Finite spectral interaction of narrow input lines with broad backscattered spectra are considered by solving numerically the nonlinear integro-differential ion-Compton equations. The results are compared to those obtained by a single wide-bandwidth input spectrum.

I. INTRODUCTION

In laser-plasma interaction experiments on inertial fusion devices, where a long-scale-length plasma surrounds the target,[1] or in the propagation of laser signals through a long optical fiber,[2] stimulated Brillouin backscattering (SBS) may be an important problem, since it is capable of reflecting a large fraction of the laser energy.[3] Among several already proposed mechanisms for limiting SBS,[4] the author has recently suggested to use suitable multiline input spectra where the separation between the lines resonantly forces or drives stimulated Brillouin rescattering.[5] Indeed, if the plasma or the nonlinear optical medium is stationary, the parametric instability between the incident laser wave I_1 of frequency ω_1 and wave vector $\mathbf{k}_1$ and the forward-traveling ion-acoustic wave I_{s+} of frequency $\omega_{s+}=k_{s+}c_s$ and wave vector $\mathbf{k}_s=2\mathbf{k}_1$, drives a backscattered downshifted wave I_2 of frequency $\omega_2=\omega_1-\omega_{s+}$ and wave vector $\mathbf{k}_2=\mathbf{k}_1-\mathbf{k}_{s+}$. An additional input satellite line $I_3(\omega_2=\omega_1-2\omega_s)$, twice ω_s downshifted with respect to I_1, may interact with the once ω_s downshifted backscattered light $I_2(\omega_2=\omega_1-\omega_s)$ by the symmetric three-wave parametric interaction with the backward-traveling acoustic wave $I_{s-}(\omega_3=\omega_2-\omega_{s-};\mathbf{k}_3=\mathbf{k}_2-\mathbf{k}_{s-})$. This rescattering process enhances I_3 due to the repeated reflection of I_1. In a finite medium of length L, small values of the satellite on the main input intensity rate I_3/I_1, are enough for the repeated reflection of a large fraction of the light intensity and therefore a strong reduction of reflection loss.[5] The separation between the lines could be greater if the same mechanism is applied to an inhomogeneous and supersonic flowing plasma.[6] Natural rescattering of the single-pump pulse has already been investigated,[7] but it is not an effective process for small noise levels because the rescattered wave must grow from a small amplitude noise as it propagates in the direction of decreasing backscattered intensity.

This mechanism, due to specific spectral separation between the lines is different from the classical multiline input spectrum effect,[4,8–10] where the difference between the frequencies must be simply greater than the Brillouin backscatter growth rate γ in order to interact each line independently of the other. Here, assuming strong damping of the ion-acoustic waves, we shall consider a four EM mode model for the evolution of the pump intensities I_1 and I_3 and of the backward stimulated intensities I_2 and I_4. The steady state is analytically solved and an explicit formula for the reflection coefficient R is exhibited which generalizes Tang's formula[11] for only one pump intensity. The coherent model may be directly derived from the complete set of coherent equations for the electric fields E_i herein called the "weak coupling case" [$\gamma<(c_s/c)\omega_s$ where c_s is the ion-acoustic velocity]. In the opposite situation, [$\gamma\gg(c_s/c)\omega_s$] which we call the "strong coupling case," we conclude that the derivation of the intensity equations is only justified within the random-phase approximation for the fields, even if very recent numerical results of the dynamical evolution of the complete coherent set of equations seem to show similar stationary regimes (cf. comments in Appendix B). In the heavy ion-damping limit we shall consider here[11] ($\gamma_s\gtrsim\omega_s$; $ZT_e\sim T_i$), the SBS parametric instability is convective[12] and merges to stimulated ion-Compton scattering.[13,14] The backscattered radiation which was downshifted by the acoustic frequency

$$\omega_s=k_s c_s \simeq k_s[(2k_B T_e+3k_B T_i)/m_i(1+k_s^2\lambda_D^2)]^{1/2}$$

becomes now downshifted by the ion-Doppler width

$$\Delta\omega_D=2(k_B T_i/m_i c^2)^{1/2}\omega_L ,$$

where $\omega_L=2\pi c/\lambda_L$ is the pump frequency and the backscatter growth rate is given by[5,13,15]

$$\gamma=10^{-7}n_e\lambda_L^3\beta_i[I_L/(1\ \mathrm{W/cm^2})]/[T_i/(1\ \mathrm{eV})] , \quad (1)$$

where

$$\beta_i = |\chi_e|^2/|1+\chi_e+\chi_i|^2 ,$$

$\chi_{e,i}$ being the electron and ion susceptibilities. Finite spectral interaction of narrow input lines with broad backscattered spectra are considered in the frame of nonlinear ion-Compton scattering. The limitation of reflection is somewhat decreased but the qualitative effect still remains. Finally, these driven stimulated Brillouin rescattering results are compared to those obtained by the input of a broad spectrum of the same intensity. Finite spectral-bandwidth ($\delta\omega$) interaction increases the gain length and has been proposed as an efficient mechanism for limiting SBS in long-scale-subcritical plasmas.[1,4,12,15,16] Thomson[16] has considered a broad-bandwidth effect ($\delta\omega \gg \gamma$) as an important stabilizing effect for both absolute and convective instabilities. Starting from the coherent equations and within the linear parametric approximation for backscattering, he has modeled the bandwidth by a Kubo-Anderson process and exhibits thresholds and growth rates in order to stabilize SRS (stimulated Raman scattering) and SBS in laser-fusion experiments. His model is only valid for $\delta\omega \gg \gamma$, where γ is the growth rate and cannot describe situations of moderate spectral bandwidth $\delta\omega \lesssim \gamma$, which are those considered here. His conclusion is that a relative bandwidth $\delta\omega/\omega_L$ of few percent is necessary in order to stabilize stimulated reflection. Here, I solve numerically the stimulated ion-Compton integro-differential equations governing nonlocal spectral interaction and nonlinear pump depletion—regardless of the specific spreading mechanism—and I show that moderate spectral bandwidths are enough to significantly lower stimulated reflection, the limitation being important for $\delta\omega \sim \gamma_s \sim \Delta\omega_D$, where $\Delta\omega_D$ is the ion-Doppler width.

II. INTENSITY MODEL EQUATIONS

We consider a finite, one-dimensional, homogeneous plasma slab of length L. A forward high-frequency electromagnetic pump wave $E_1(k_1,\omega_1)$ decays parametrically into a forward-traveling ion-acoustic wave $E_{s+1}(k_{s+1},\omega_{s+1})$ and a backscattered electromagnetic wave $E_2(k_2=-(k_1-k_{s+1}),\omega_2=\omega_1-\omega_{s+1})$ and exhibits pump depletion. In the case of damped acoustic waves, this well-known three-wave interaction has already been considered[11,17] and the equations analytically integrated in the heavy ion-damping limit.[18] Now, we allow further decay. The backscattered wave E_2 may interact with the driven electromagnetic pump wave $E_3(k_3=-(k_2-k_{s-}),\omega_3=\omega_2-\omega_s)$ and a backward-traveling ion-acoustic wave $E_{s-}(k_{s-},\omega_{s-})$ by the symmetric three-wave process. Finally, since the intensity of the satellite pump wave E_3 may be high enough to overcome threshold, it can also be depleted into a backscattered electromagnetic wave $E_4(k_4=-(k_3-k_{s+2}),\omega_4=\omega_3-\omega_{s+2})$ and a forward-traveling ion-acoustic wave $E_{s+2}(k_{s+2},\omega_{s+2})$. The three-wave equations are readily generalized to cover the present six-wave interaction[13,19]

$$(\partial_t+c\partial_x+\gamma_1)E_1=-KE_2E_{s+} , \tag{2}$$

$$(\partial_t+c_s\partial_x+\gamma_s)E_{s+} = K^*\{E_1E_2^*+E_3E_4^*\exp[i\,\Delta\omega(t-x/c_s)]\} , \tag{3}$$

$$(\partial_t-c\partial_x+\gamma_2)E_2=K^*(E_1E_{s+}^*-E_3E_{s-}) , \tag{4}$$

$$(\partial_t-c_s\partial_x+\gamma_s)E_{s-}=KE_2E_3^* , \tag{5}$$

$$(\partial_t+c\partial_x+\gamma_3)E_3 = K\{E_2E_{s-}^*-E_4E_{s+}\exp[-i\,\Delta\omega(t-x/c_2)]\} , \tag{6}$$

$$(\partial_t-c\partial_x+\gamma_4)E_4=K^*E_3E_{s+}^*\exp[i\,\Delta\omega(t-x/c_s)] , \tag{7}$$

where K is the coupling constant[12,13] and $\Delta\omega$ is the frequency mismatch obtained from the resonant relations between the electric fields $E_i \propto \exp[i(k_jx-\omega_jt)]$, $j=s+1,s-,s+2,1,2,3,4$:

$$\omega_1-\omega_2=(k_1-k_2)c=\omega_{s+1}=k_{s+1}c_s , \tag{8}$$

$$k_{s+1}=k_1+k_2\simeq 2k_1(1-c_s/c) , \tag{9}$$

$$k_1-k_2=2k_1(c_s/c)(1-c_s/c) , \tag{10}$$

$$\omega_2-\omega_3=(k_2-k_3)c=\omega_{s-}=k_{s-}c_s , \tag{11}$$

$$k_{s-}=k_2+k_3\simeq 2k_1(1-3c_s/c) , \tag{12}$$

$$k_2-k_3=2k_1(c_s/c)(1-3c_s/c) , \tag{13}$$

$$\omega_3-\omega_4=(k_3-k_4)c=\omega_{s+2}=k_{s+2}c_s , \tag{14}$$

$$k_{s+2}=k_3+k_4\simeq 2k_1(1-5c_s/c) , \tag{15}$$

$$k_3-k_4=2k_1(c_s/c)(1-5c_s/c) . \tag{16}$$

The forward-traveling ion-acoustic wave is driven by the ponderomotive potential resulting from the beat between E_1 and E_2 and between E_3 and E_4,

$$\begin{aligned}E_{s+}&=E_{s+1}\exp[i(k_{s+1}x-\omega_{s+1}t)]+E_{s+2}\exp[i(k_{s+2}x-\omega_{s+2}t)]\\&=\exp[2ik_1(1-c_s/c)(x-c_st)]\{E_{s+1}+E_{s+2}\exp[i\,\Delta\omega(t-x/c_s)]\}\end{aligned} \tag{17}$$

where $\Delta\omega$ is obtained from relations (8), (9), (14), and (15)

$$\Delta\omega=\omega_{s+1}-\omega_{s+2}=8k_1c_s^2/c=4(c_s/c)\omega_s , \tag{18}$$

ω_s being the mean ion-acoustic frequency.

In the heavy ion-damping limit ($\gamma_s \rangle |\partial_t+c_s\partial_x| \sim\gamma$) and nondamped EM waves ($\gamma_i=0,i=1,4$) Eq. (3) yields

$$E_{s+}=(K^*/\gamma_s)[E_1E_2^*+E_3E_4^*\exp(i\phi)] , \tag{19}$$

where $\phi=\Delta\omega(t-x/c_s)$. The characteristic evolution time for the field amplitudes E_i is given by $\gamma=|KE_1|^2/\gamma_s$. In the weak coupling case ($\Delta\omega>\gamma$) the forward-traveling ion-acoustic wave E_{s+} can be shared into two well-separated waves E_{s+1} and E_{s+2}, respectively driven by (E_1,E_2) and (E_3,E_4), since the acoustic frequencies ω_{s+1} and ω_{s+2} are distinct. Instead of Eq. (3) for E_{s+} we can write two equations for E_{s+1} and E_{s+2},

$$E_{s+1}=(K^*/\gamma_s)E_1E_2^* , \tag{20}$$

$$E_{s+2}=(K^*/\gamma_s)E_3E_4^*\exp(i\phi) , \tag{21}$$

and an equation for the backward-traveling acoustic field E_{s-},

$$E_{s-}=(K/\gamma_s)E_2E_3^* . \tag{22}$$

Substituting Eqs. (20) and (22) into Eqs. (2) and (4) and Eqs. (21) and (22) into Eqs. (6) and (7), and multiplying by the respective complex conjugate amplitudes, we obtain four coupling Volterra equations for the intensities $I_i=(2/\gamma_s)\,|KE_i\,|^2$, namely,

$$(\partial_t+c\partial_x)I_1=-I_1I_2 , \tag{23}$$

$$(\partial_t-c\partial_x)I_2=I_2(I_1-I_3) , \tag{24}$$

$$(\partial_t+c\partial_x)I_3=I_3(I_2-I_4) , \tag{25}$$

$$(\partial_t-c\partial_x)I_4=I_3I_4 . \tag{26}$$

In the strong coupling case ($\Delta\omega\ll\gamma$), as we shall see, Eqs. (23)—(26) are only justified by additional assumptions on fast phase variation of the fields. Note that if E_4 is negligible, small Eqs. (2)—(7) in the heavy ion-damping limit directly lead to the Volterra system of equations for I_1, I_2, and I_3 without restrictions.[20] Numerical computation of the evolution equations (23)—(26) for two pumps I_1 and I_3 depleting into a homogeneous plasma slab of length L, with transparent boundaries, shows that the stationary regime is rapidly attained after a short time-dependent transiency of a few damped oscillations of period $\tau=2L/c$ (photon transit time). For partially reflective boundaries a feedback mechanism may produce strongly oscillatory regimes leading even to optical chaos.[20] The steady-state equations (putting $c=1$):

$$dI_1/dx=-I_1I_2 , \tag{27}$$

$$dI_2/dx=I_2(I_3-I_1) , \tag{28}$$

$$dI_3/dx=I_3(I_2-I_4) , \tag{29}$$

$$dI_4/dx=-I_3I_4 , \tag{30}$$

have invariants

$$I_1(x)-I_2(x)+I_3(x)-I_4(x)=D , \tag{31}$$

$$I_1(x)I_3(x)+I_2(x)I_4(x)-I_1(x)I_4(x)=(D/2)^2-C_2^2 , \tag{32}$$

and can be analytically integrated[5] yielding the solutions

$$I_1(x)=\frac{[(D/2)^2-C_2^2]\exp(Dx/2)\sinh[C_2(x+C_1)]}{C_3+\exp(Dx/2)\{(D/2)\sinh[C_2(x+C_1)]-C_2\cosh[C_2(x+C_1)]\}} , \tag{33}$$

$$I_2(x)=I_1(x)-D/2-C_2\coth[C_2(x+C_1)] , \tag{34}$$

$$I_3(x)=C_2^2/\{I_2(x)\sinh^2[C_2(x+C_1)]\} , \tag{35}$$

$$I_4(x)=I_1(x)-I_2(x)+I_3(x)-D , \tag{36}$$

where D, C_1, C_2, and C_3 are four integration constants which can be expressed as functions of the four boundary conditions: $I_1(0)$, $I_2(L)$, $I_3(0)$, and $I_4(L)$. The solutions (33)—(36) are plotted in Fig. 1 for a given length L and a given rate of the satellite intensity over main input intensity $a=I_3(0)/I_1(0)=0.2$. The main input line intensity $I_1(x)$ exhibits pump depletion during its forward propagation through the plasma slab, as follows from Eq. (27). The depleted intensity enhances the backscattered line $I_2(x)$ which grows in the backward direction starting with the noise intensity $I_2(L)=I_N$ at $x=L$. However, the forward propagating satellite $I_3(x)$ shows convective amplification as follows from Eq. (29). Part of the backscattered intensity I_2 is reflected again by this driven rescattering process. $I_3(x)$ stimulates also some backscattered intensity $I_4(x)$ starting from $I_4(L)=I_N$. The result is an increase of the transmissivity with respect to the single-backscattering process. The reflection coefficient defined by

$$R(L)=\frac{I_2(0)+I_4(0)}{I_1(0)+I_2(L)+I_3(0)+I_4(L)} \tag{37}$$

will be a function of the input intensities $I_1(0)$ and $I_3(0)$ for given noise $I_2(L)$ and $I_4(L)$ and a given depth L, generalizing Tang's formula[11]

$$R(L)=\frac{\exp[(1-R)LI_1(0)]}{[I_1(0)/I_2(L)](1-R)+1} \tag{38}$$

for single stimulated backscattering ($I_3=I_4=0$). From definitions,

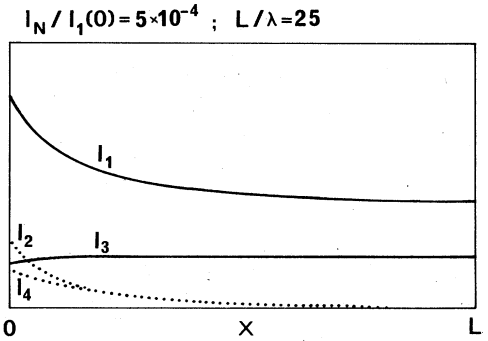

FIG. 1. Stationary solutions of the four EM mode model for the intensities. Spatial distribution in the plasma slab of length L of the incident pump intensity I_1 depleted into the stimulated backscattered intensity I_2. The driven rescattered pump intensity I_3 exhibits convective amplification during its forward propagation and stimulated again the backscattered intensity I_4.

$$X=C_2\ , \tag{39}$$

$$Y=C_2(x+C_1)\ . \tag{40}$$

Equation (37) may be written

$$R(L)=1-\frac{D+I_2(L)+I_4(L)}{I_1(0)+I_2(L)+I_3(0)+I_4(L)} \tag{41}$$

[in the following we shall put $I_1\equiv I_1(0)$, $I_2\equiv I_2(L)$, $I_3\equiv I_3(0)$, and $I_4\equiv I_4(L)$ which are the boundary known parameters], where

$$D/2=I_1-X[Y+(X/I_3)(Y^2-1)] \tag{42}$$

and where $Y=Y(X,L)$ is one analytic solution (see Appendix A) of the fourth-order algebraic equation

$$\sum_{n=0}^{4} a_n Y^n=0\ , \tag{43}$$

with coefficients

$$a_0=1\ ,$$

$$a_1=2d+I_3/X\ ,$$

$$a_2=(1+I_3/I_2)(d^2-1)+I_3[3d-(I_1+I_4)/X]/X\ ,$$

$$a_3=(I_3/X)[1+2d^2-2d(I_1+I_4)/X]-2d\ ,$$

$$a_4=(I_3/X)[X(1-d^2)/I_2+d-d^2(I_1+I_4)/X]-d^2\ ,$$

where $d=\coth XL$, and where X is determined by the equation

$$\frac{I_1I_2I_3I_4}{(d^2-1)^{1/2}}\exp(DL/2)=\frac{X^2(Y^2-1)}{Y+d}\sum_{n=0}^{4} b_nX^n\ , \tag{44}$$

with

$$b_0=(I_3-I_1)(I_1+I_4)\ ,$$

$$b_1=2(I_1+I_2)Y+(I_1-I_3)(Y^2-1)/(Y+d)\ ,$$

$$b_2=(2I_1+I_2-I_3)(Y^2-1)/I_3-2Y(Y^2-1)/(Y+d)\ ,$$

$$b_3=-[(Y^2-1)/I_3][(Y^2-1)/(Y+d)+2Y]\ ,$$

$$b_4=-[(Y^2-1)/I_3]^2\ ,$$

which is easily solved by Newton's method. The results are plotted in Figs. 2 and 3. In Fig. 2 the reflection coefficient R is plotted versus the two-line input ratio $a=I_3(0)/I_1(0)$ for three values of the "quality factor" $Q=LI_1(0)$ which stands for the number of linear growth lengths for SBS in a homogeneous plasma of length L, namely,[21]

$$Q=\frac{\pi}{2}\frac{L}{\lambda}\frac{n_e}{n_c}\frac{\epsilon_0E_1^2}{n_ck_BT_e}\frac{\omega_s}{\gamma_s}\left[1+\frac{3T_i}{ZT_e}\right]^{-1}\left[1-\frac{n_e}{n_c}\right]^{-1}.$$

Here $I_1(0)=I_L$ is the incident intensity at $x=0$ and $I_2(L)=I_4(L)=I_N$ is the intensity of the noise in the backscattered waves at $x=L$. We have taken $I_N/I_L=5\times10^{-4}$. As we can see for a given ratio $a<1$,

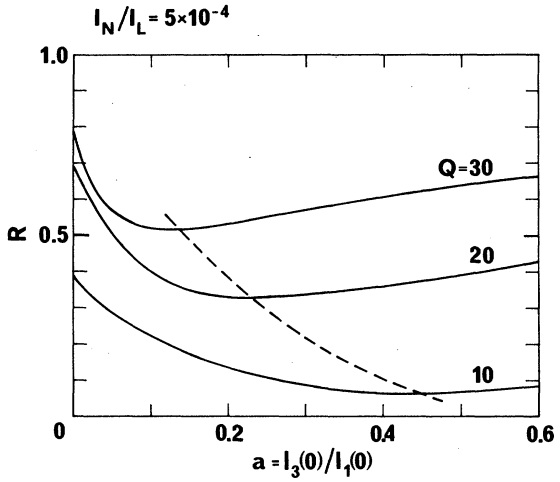

FIG. 2. Reflection coefficient $R=(I_2+I_4)/(I_1+I_3)$ versus the satellite on main input intensity rate $a=I_3(0)/I_1(0)$ for three values of the quality factor Q (or depth L). The dashed curve is the locus of the reflectivity minima. The main EM input intensity $I_1(0)=I_L$ is kept constant over noise intensity $I_N=I_2(L)=I_4(L)$, namely $I_N/I_L=5\times10^{-4}$.

the reflectivity R presents a minimum value which is considerably lower than the single-scattering value ($a=0$). These minima are represented by the dashed curve. In Fig. 3, we plot the reflectivity R versus the quality factor Q [or the depth L for a given input intensity $I_1(0)=I_L$]. We show comparatively the steady state of the following:

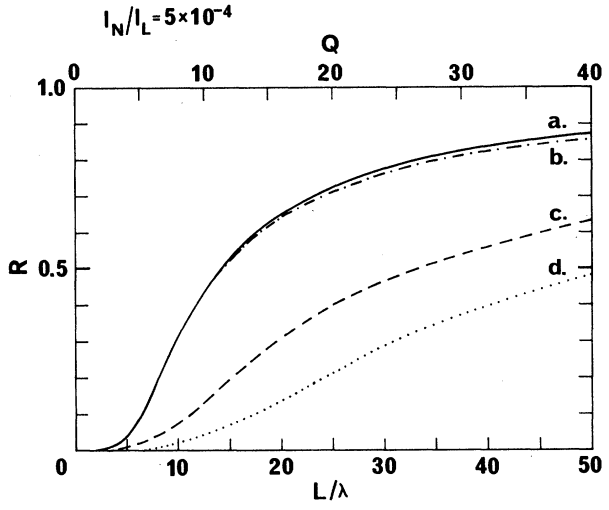

FIG. 3. Reflectivity R versus the quality factor Q (or the depth L) for constant main input intensity $I_1(0)=I_L$ over noise I_N. Steady-state reflectivity of the following: (a) two-mode single-scattering [Tang (Ref. 11) Eq. (38)] (solid curve); (b) three-mode natural rescattering [Speziale *et al.* (Ref. 7)] (dot-dashed curve); (c) four-mode driven rescattering, Eq. (30) (dashed curve) for a relative satellite intensity $a=I_3(0)/I_1(0)=0.2$; (d) six-mode driven rescattering, Eqs. (45) and (46) (dotted curve) with two input satellites $I_3(0)$ and $I_5(0)$ satisfying $I_3(0)/I_1(0)=I_5(0)/I_3(0)=0.2$.

(a) the two-mode single scattering[11] given by formula (38) (solid curve);

(b) the three-mode natural rescattering[7] where the rescattered light grows from the noise level $I_3(0)=I_N$ (dot-dashed curve), which does not differ significantly from the single-scattering case;

(c) the four-mode driven rescattering given by formula (41) (dashed curve) where a satellite of relative intensity $a=0.2$ has been added, leading to a net reduction of the reflectivity; and,

(d) the six-mode driven rescattering (dotted curve) where a second satellite $I_5(0)$ has been added to first $I_3(0)$, twice ω_s downshifted with respect to it, in order to further reduce the reflectivity. Relative intensities

$$I_3(0)/I_1(0)=I_5(0)/I_3(0)=0.2$$

are sufficient to obtain this further diminution of R.

Such a three-line input spectrum has been numerically treated by the following set of six equations[5]

$$(\partial_t+c\partial_x)I_{2j-1}(x,t)=I_{2j-1}(x,t)[I_{2j-2}(x,t)-I_{2j}(x,t)] , \tag{45}$$

$$(\partial_t-c\partial_x)I_{2j}(x,t)=I_{2j}(x,t)[I_{2j-1}(x,t)-I_{2j+1}(x,t)] , \tag{46}$$

where $2j=1=1,3,5$ stands for the forward input lines and $2j=2,4,6$ stands for the backscattered lines, and where $I_0=I_7=0$ closes the system.

In the strong coupling case ($\Delta\omega\ll\gamma$) we can put $\Delta\omega=0$ in Eqs. (2)—(7), and substituting E_{s+} from Eq. (19), for $\phi=0$, Eqs. (3), (4), (6), and (7) yield

$$(\partial_t+c\partial_x)E_1=(|K|^2/\gamma_s)(-E_1|E_2|^2-E_2E_3E_4^*) , \tag{47}$$

$$(\partial_t-c\partial_x)E_2=(|K|^2/\gamma_s)[E_2(|E_1|^2-|E_3|^2)+E_1E_3^*E_4] , \tag{48}$$

$$(\partial_t+c\partial_x)E_3=(|K|^2/\gamma_s)[E_3(|E_2|^2-|E_4|^2)-E_1E_2^*E_4] , \tag{49}$$

$$(\partial_t-c\partial_x)E_4=(|K|^2/\gamma_s)(E_4|E_3|^2+E_1^*E_2E_3) . \tag{50}$$

We can multiply each equation by the respective complex conjugate field but the last right-hand-side terms prevent one from obtaining the Volterra intensity, equations (23)—(26), since they couple together the amplitudes a_i and the phases φ_j of the fields $E_j=a_j\exp(i\varphi_j)$. In order to neglect these terms we must moreover assume a rapid random variation of the phases φ_j. Thus we rejoin the random-phase approximation where the Volterra intensity equations are naturally derived from the integro-differential equations, as we shall see in Sec. III. Otherwise, we obtain six couple equations for the amplitudes a_1, a_2, a_3, and a_4 and for two phase functions $\varphi=\varphi_1+\varphi_4-(\varphi_2+\varphi_3)$ and $\psi=\varphi_1+\varphi_2-(\varphi_3+\varphi_4)$ (see Appendix B).

III. FINITE-BANDWIDTH SPECTRAL INTERACTION

In the heavy ion-damping case ($\gamma_s\sim\omega_s$) we deal with here, the backscattered spectra are broad ($\delta\omega\sim\gamma_s$) and their spectral interaction with the input narrow lines ($\delta\omega\ll\omega_s$) can reduce the driven stimulated rescattering process. In order to evaluate this effect and to compare these multiline results to those due to a broad ($\delta\omega\sim\omega_s$) input spectrum, we solve the kinetic equations governing nonlinear ion-Compton scattering.[13–15,22] The couple of integro-differential equations governing the one-dimensional, nonlocal and nonlinear counterpropagation of the incident photon spectrum $N_+(\omega,x,t)$ and the stimulated backscattered photon spectrum $N_-(\omega,x,t)$ are given by[15]

$$(\partial_t+c\partial_x)N_+(\omega,x,t)=N_+(\omega,x,t)\int d\omega'\,W(\omega,\omega')N_-(\omega',x,t) , \tag{51}$$

$$(\partial_t-c\partial_x)N_-(\omega,x,t)=N_-(\omega,x,t)\int d\omega'\,W(\omega,\omega')N_+(\omega',x,t) , \tag{52}$$

where[22]

$$N_\pm(\omega,x,t)=[\pi^2/(2\hbar\omega^2)]\partial_\omega\omega^2\epsilon^t(\omega,t)|E_\pm(k,x,t)|^2 , \tag{53}$$

$\epsilon^t(\omega,k)$ being the dielectric function entering the transverse dispersion relation $k^2c^2=\omega^2\epsilon^t(\omega,k)$ and where the interaction kernel is given by

$$W(\omega,\omega')=W_0[(\omega'-\omega)/\Delta\omega_D]\times\exp\{-[(\omega-\omega')/\Delta\omega_D]^2\} , \tag{54}$$

the transition probability W_0 being proportional to the Thomson scattering cross section $\sigma_T=(8\pi/3)(e^2/m_ec^2)^2$ and function of the electron and ion susceptibilities

$$\chi_{e,i}(\omega_-,k_-)=\frac{\omega_{Pe,i}^2}{k_-^2}\int d^3v\frac{\mathbf{k}_-\cdot\partial f_{e,i}/\partial\mathbf{v}}{\omega_--\mathbf{k}_-\cdot\mathbf{v}} , \tag{55}$$

by means of

$$W_0=\frac{3n_e\hbar c\sigma_T}{(2\pi)^3k_BT_i}\frac{|\chi_e|^2}{|1+\chi_e+\chi_i|^2} , \tag{56}$$

where n_e is the electron density, T_i is the ion temperature, and $\Delta\omega_D$ is the ion-Doppler width associated with backscattering

$$\Delta\omega_D=2(2k_BT_i/m_ic^2)^{1/2}\omega . \tag{57}$$

Equations (51) and (52) do not take into account the ion dynamics which has the effect of increasing the ion tem-

perature[23] and therefore of reducing the probability W_0. Here we are only interested in spectral effects. Equations (51) and (52) lead therefore to the $2n$ Volterra equations (45) and (46) for the electromagnetic intensities if we assume the spectra composed of narrow lines

$$N_+(\omega) \propto \sum_{j=1}^{n} \delta(\omega-\omega_{2j-1}) , \tag{58}$$

$$N_-(\omega) \propto \sum_{j=1}^{n} \delta(\omega-\omega_{2j}) , \tag{59}$$

separated each one from the other by $\Delta\omega_D/\sqrt{2}$. In general, we solve Eqs. (51) and (52) numerically for a multicomponent input spectrum $N_+(\omega,x,t)$ composed of a superposition of Gaussian spectra

$$N_i \exp\{-[(\omega-\omega_i)/\delta\omega]^2\}$$

of width $\delta\omega$ separated from each other by $2(\Delta\omega_D/\sqrt{2})$. The steady-state spectra are plotted in Figs. 4 and 5. Figure 4 corresponds to the finite spectral interaction of a two-line input spectrum [one satellite $N_3(\omega)$], each line of relative width $\delta\omega/\Delta\omega_D=0.1$. The figure shows the ingoing spectra at $x=0$ (solid curves) and the outgoing spectra at $x=L$ (dashed curves). The nonlinear ion-Compton interaction stimulate broad backscattered spectra $N_2(\omega)$ and $N_4(\omega)$ (dotted curves).

The line intensities $I_i=c\int d\omega N_i(\omega)$ satisfy $I_3(0)/I_1(0)=0.2$. In Fig. 5 we show comparatively the steady-state spectra for the single-backscattering case (upper graph of Fig. 5), the two-line input spectrum case (middle graph of Fig. 5) where 20% additional intensity is carried by a first satellite (Fig. 4), and the three-line input spectrum case (lower graph of Fig. 5) with additional intensity on two satellites satisfying

$$I_3(0)/I_1(0)=I_5(0)/I_3(0)=0.2 .$$

We can verify the diminution of the reflectivity by reading the value of the reflection coefficient R shown in each figure, for two depths or quality factors $Q=20$ (dotted backscattered spectra) and $Q=36$ (dashed backscattered spectra) and a constant value of the noise over main input line intensity rate $I_N/I_1(0)=5\times10^{-4}$. We assume that the spectral interaction builds up from a wide constant noise spectrum, which is able to propagate photon soliton structures in unbounded homogeneous media.[24]

Finally, we compare these results to the stimulated reflection produced by a single input spectrum of the same intensity $I_N/I_L=5\times10^{-4}$, where the relative spectral bandwidth $\rho=\delta\omega/\Delta\omega_D$ varies from $\rho=0$ [fine-line spectrum described by Tang's formula (38)] to $\rho=2$ (rather wide-bandwidth spectrum). We maintain $\Delta\omega_D$ constant, i.e., the ion temperature T_i, in order to keep the same probability (56) and we vary $\delta\omega$. As we can see in Figs. 6–8, this limitation mechanism for stimulated reflection, based on the convolution property of integral equations (51) and (52), is very efficient. When the ingoing spectrum, $N_+(\omega)$, has a bandwidth comparable to the Doppler width, $\Delta\omega_D$ of the antisymmetric Compton kernel $W(\omega,\omega')$ expressed in (54), overlapping of the counter-

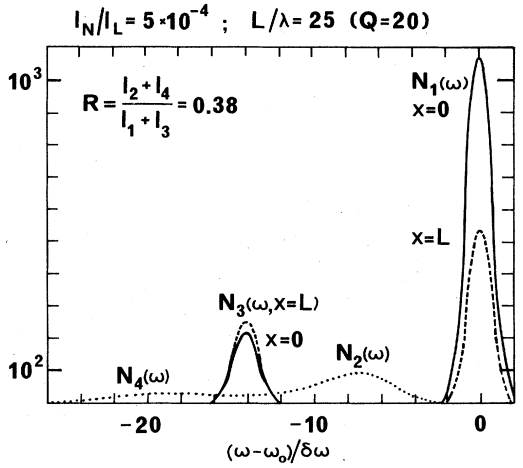

FIG. 4. Finite-bandwidth spectral interaction due to stimulated ion-Compton backscattering of a two-line $N_1(\omega)$ and $N_3(\omega)$ input spectrum each line of narrowness $\delta\omega/\Delta\omega_D=0.1$: ingoing spectra $N_1(\omega,0)$ and $N_3(\omega,0)$ at $x=0$ (solid curves) and outgoing spectra $N_1(\omega,L)$ and $N_3(\omega,L)$ at $x=L$ (dashed curves). The nonlinear interaction stimulates broad backscattered spectra $N_2(\omega)$ and $N_4(\omega)$ (dotted curves). The line intensities $I_i=c\int d\omega N_i(\omega)$ satisfy $I_3(0)/I_1(0)=0.2$.

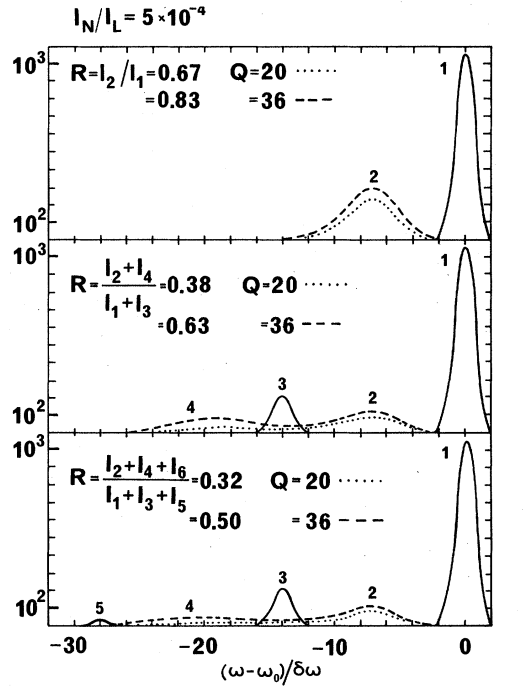

FIG. 5. Steady-state spectra with finite-bandwidth interaction: (upper graph) single-backscattering case; (middle graph) two-line input spectrum (Fig. 4) with satellite relative intensity $I_3(0)/I_1(0)=0.2$; (lower graph) three-line input spectrum with additional intensity on two satellites satisfying $I_3(0)/I_1(0)=I_5(0)/I_3(0)=0.2$. Reflectivity values shown on each graph for two quality factors $Q=20$ (dotted backscattered spectra) and $Q=36$ (dashed backscattered spectra). Constant main input line intensity $I_1(0)=I_L$ over noise I_N: $I_N/I_L=5\times10^{-4}$.

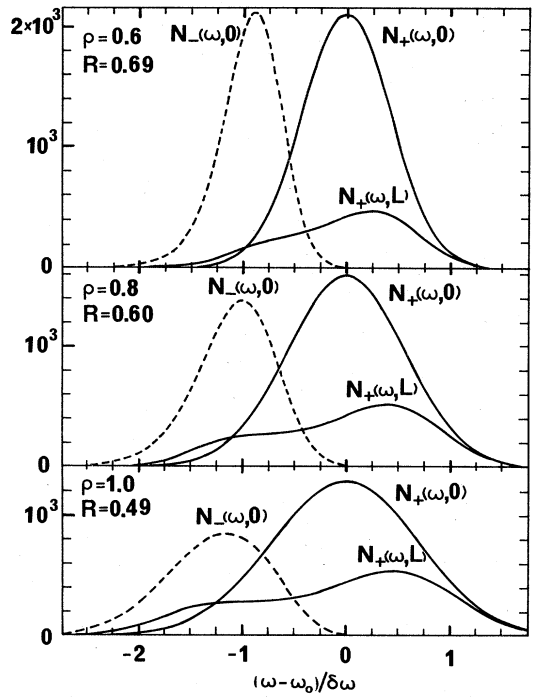

FIG. 6. Wide-bandwidth spectral interaction for the single-scattering case. Steady-state spectra for three values of the relative width $\rho=\delta\omega/\Delta\omega_D$, keeping constant the Doppler width $\Delta\omega_D$ which ensures the same ion temperature T_i and the same transition probability W_0. Reflectivity values shown on each graph.

streaming spectral wings reduces the backscatter instability growth rate. Even if in this heavy ion-damped case the resonance width has a less precise meaning, we can physically understand the decrease of efficiency by looking at Fig. 6. The intensity of the pump $N_+(\omega)$ is dispersed over a frequency range $\delta\omega$, while only that around the maximum of $N_+(\omega)$ ("resonant region") is situated at the "resonant distance $\Delta\omega_D/\sqrt{2}$" and can effectively drive

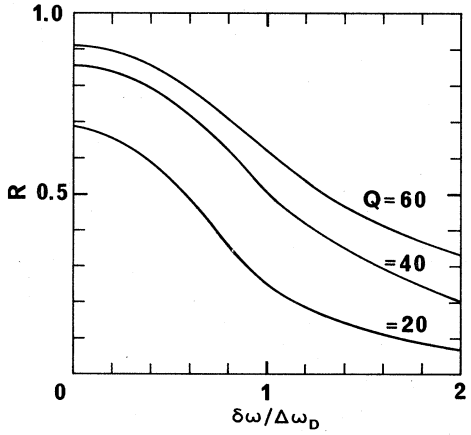

FIG. 7. Finite-bandwidth spectral interaction: reflectivity R versus relative bandwidth $\rho=\delta\omega/\Delta\omega_D$ for the single-scattering case.

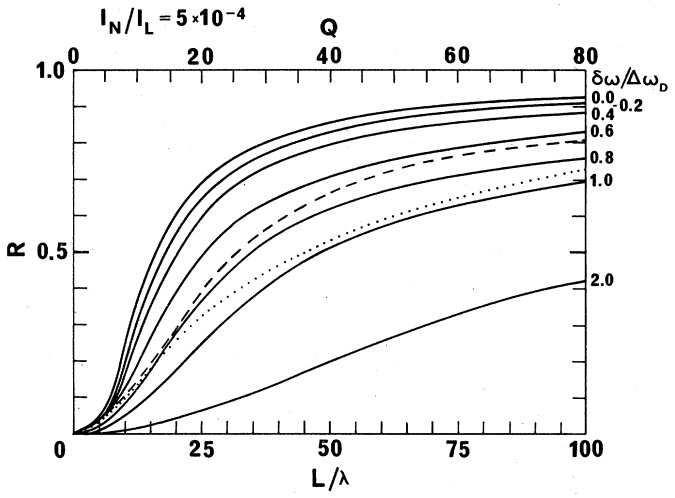

FIG. 8. Reflectivity versus plasma depth L/λ or quality factor Q: single-scattering interaction (solid curves) for different relative bandwidth $\rho=\delta\omega/\Delta\omega_D$. Also plotted are the driven rescattering results of the two narrow ($\rho=0.1$) line input spectrum of Fig. 4 or the middle graph of Fig. 5 (dashed curve) and of the three-line input spectrum of lower graph of Fig. 5 (dotted curve).

the backscatter instability. As we can read in Fig. 6, a small increase of the relative width $\rho=\delta\omega/\Delta\omega_D$ appreciably reduces the reflectivity R. The diminution over the range $0<\rho<2$ is plotted in Fig. 7 for three depths L or quality factors Q. In Fig. 8, the reflection coefficient $R=I_-(0)/I_+(0)$ is plotted versus plasma depth L/λ or quality factor Q for typical laser-plasma parameters. From (1) the characteristic growth length of the convective instability is $x_c=5\lambda/4$ for a CO_2 laser-plasma interaction of $I_L=10^{13}$ W/cm^2, $n_e=10^{19}$ cm^{-3}, and $T_e=T_i=1$ keV. The single-scattering interaction is represented by the solid curves for different values of $\rho=\delta\omega/\Delta\omega_D$. We also plot in Fig. 8 the driven rescattering results of the two narrow ($\rho=0.1$) line input spectrum of Fig. 4 or the middle graph of Fig. 5 (dashed curve) and those due to the three-line input spectrum of the lower graph of Fig. 5 (dotted curve). As we can infer, for $\rho\gg1$, we rejoin Thomson's result.[16]

IV. CONCLUSION

Both, driven stimulated rescattering and finite-bandwidth spectral interaction are candidate mechanisms for limiting reflection due to convective stimulated Brillouin backscattering from long-scale-length plasmas[1] or from long nonlinear optical media[2] in the heavy-ion damping case. However, the second spectral shape seems more efficient inasmuch as moderate spectral bandwidths lead to the same result as an additional 20% intensity on a twice ω_s downshifted satellite line. It will depend on the physical situation that one mechanism is preferable to the other. In laser-fusion experiments, it seems more feasible to input a wide-bandwidth spectrum even if the flowing of inhomogeneous plasma renders the separation between the lines of the multicomponent spectrum less stringent and

therefore the multiline input spectrum more attractive.[6] When the goal is to transmit narrow signals by means of optical fibers or another optical material, driven stimulated rescattering by the addition of satellite lines seems an interesting mechanism to increase the transmissivity. Spreading of the input spectrum into two or many peaks may be obtained by self-phase modulation of the single input spectrum through an optical material with an intensity-dependent refractive index.[25] The frequency shift depends on the input intensity and on the pulse duration.

ACKNOWLEDGMENTS

I thank D. Pesme and J. Coste for valuable discussions. The contribution of J. Peyraud in numerical calculations is acknowledged too.

APPENDIX A

The fourth-order algebraic equation (43) may be transformed into the following equation without cubic term

$$Z^4+aZ^2+bZ+c=0 \tag{A1}$$

by the change

$$Y=Z-\frac{a_1}{4} , \tag{A2}$$

where the coefficients are given by

$$a=a_2-\tfrac{3}{8}a_1^2 ,$$
$$b=a_3-\tfrac{1}{2}a_1a_2+\tfrac{1}{8}a_1^3 ,$$
$$c=a_4-\tfrac{1}{4}a_1a_3+\tfrac{1}{16}a_2a_1^2-\tfrac{3}{256}a_1^2 .$$

Now, Eq. (A1) may be factorized into a product of two quadratic equations[26]

$$Z^4+aZ^2+bZ+c=(Z^2+\zeta Z+\eta)(Z^2-\xi Z+\zeta) =0 , \tag{A3}$$

where

$$a=\eta+\zeta+\xi^2 , \quad b=\xi(\zeta-\eta) ,$$

and $c=\eta\zeta$ yield

$$\eta=\frac{1}{2}\left[a+\xi^2-\frac{b}{\xi}\right] ,$$
$$\zeta=\frac{1}{2}\left[a+\xi^2+\frac{b}{\xi}\right] ,$$

and where $u=\xi^2$ is the solution of the cubic equation

$$u^3+2au^2+(a^2-4c)u-b^2=0 \tag{A4}$$

which may be solved by standard methods after putting

$$p=2a ,$$
$$q=a^2-4c ,$$
$$r=-b^2 ,$$
$$A=\tfrac{1}{3}(3q-p^2) ,$$
$$B=\tfrac{1}{27}(2p^3-9pq+27r) .$$

We look for the real root

$$u=u_1+u_2-\frac{p}{3}=\xi^2 , \tag{A5}$$

where

$$u_1=\left[-\frac{B}{2}+\left[\frac{B^2}{4}+\frac{A^3}{27}\right]^{1/2}\right]^{1/3} ,$$
$$u_2=\left[-\frac{B}{2}-\left[\frac{B^2}{4}+\frac{A^3}{27}\right]^{1/2}\right]^{1/3} .$$

Substituting η, ζ, and ξ into (A3) we obtain four solutions for Z, but the physical one is given by

$$Z=\frac{\xi+(\xi^2-4\zeta)^{1/2}}{2} , \tag{A6}$$

and from (A2)

$$Y=Z-\frac{a_1}{4} .$$

APPENDIX B

By defining

$$(|K|/\sqrt{\gamma_s})E_j=a_j\exp(i\varphi_j) , \tag{B1}$$

where a_j are the real amplitudes and φ_j are the phases, the system of equations (47)—(50) for the complex fields E_j yield

$$(\partial_t+c\partial_x)a_1\exp(i\varphi_1)=-a_2^2a_1\exp(i\varphi_1)-a_2a_3a_4\exp[i(\varphi_2+\varphi_3-\varphi_4)] , \tag{B2}$$
$$(\partial_t-c\partial_x)a_2\exp(i\varphi_2)=(a_1^2-a_3^2)a_2\exp(i\varphi_2)+a_1a_3a_4\exp[i(\varphi_1+\varphi_4-\varphi_3)] , \tag{B3}$$
$$(\partial_t+c\partial_x)a_3\exp(i\varphi_3)=(a_2^2-a_4^2)a_3\exp(i\varphi_3)-a_1a_2a_4\exp[i(\varphi_1+\varphi_4-\varphi_2)] , \tag{B4}$$
$$(\partial_t-c\partial_x)a_4\exp(i\varphi_4)=a_3^2a_4\exp(i\varphi_4)+a_1a_2a_3\exp[i(\varphi_2+\varphi_3-\varphi_1)] . \tag{B5}$$

The system of four complex equations (B2)—(B5) yield eight equations for the amplitudes a_j and the phase φ_j. By defining

$$\varphi=\varphi_1+\varphi_4-(\varphi_2+\varphi_3)\ , \tag{B6}$$

$$\psi=\varphi_1+\varphi_2-(\varphi_3+\varphi_4)\ , \tag{B7}$$

and combining the equations for the phase evolutions we obtain six evolution equations which couple the amplitudes and the phases φ and ψ, namely,

$$(\partial_t+c\partial_x)a_1=-a_2^2a_1-a_2a_3a_4\cos\varphi\ , \tag{B8}$$

$$(\partial_t-c\partial_x)a_2=(a_1^2-a_3^2)a_2+a_1a_3a_4\cos\varphi\ , \tag{B9}$$

$$(\partial_t+c\partial_x)a_3=(a_2^2-a_4^2)a_3-a_1a_2a_4\cos\varphi\ , \tag{B10}$$

$$(\partial_t-c\partial_x)a_4=a_3^2a_4+a_1a_2a_3\cos\varphi\ , \tag{B11}$$

$$\partial_t\varphi+c\partial_c\psi=\sin\varphi\left[\frac{a_1a_2a_4}{a_3}+\frac{a_2a_3a_4}{a_1}-\frac{a_1a_2a_3}{a_4}-\frac{a_1a_3a_4}{a_2}\right]\ , \tag{B12}$$

$$\partial_t\psi+c\partial_x\varphi=\sin\varphi\left[\frac{a_1a_3a_4}{a_2}+\frac{a_1a_2a_4}{a_3}+\frac{a_2a_3a_4}{a_1}+\frac{a_1a_2a_3}{a_4}\right]\ . \tag{B13}$$

An additional assumption on fast variation of φ is needed in order to neglect the last terms of the right-hand side of Eqs. (B8)—(B11) and thus to obtain the intensity Volterra equations (23)—(26). This could be the case if the phases φ_j exhibit rapid random-phase approximation (RPA) variations. In the general case the complete set of Eqs. (B8)—(B13) must be solved. Very recent numerical results of the dynamical evolution of Eqs. (B8)—(B13) show stationary regimes similar to that shown in Fig. 1 for an interaction length $L<L_{\rm crit}$ and nonstationary regimes similar to those of Ref. 15 (1981) and of Ref. 20 for $L>L_{\rm crit}$.

---

*Laboratoire No. 190 Associé au Centre National de la Recherche Scientifique.

[1]D. G. Colombant, W. N. Manheimer, and J. H. Gardner, Phys. Fluids **26**, 3146 (1983).

[2]D. Cotter, J. Opt. Comm. **4**, 10 (1983).

[3]M. N. Rosenbluth, Phys. Rev. Lett. **29**, 565 (1972); D. Pesme, G. Laval, and R. Pellat, *ibid.* **31**, 203 (1973); M. N. Rosenbluth, R. B. White, and C. S. Liu, *ibid.* **31**, 1190 (1973).

[4]K. Estabrook, J. Harte, E. M. Cambell, F. Ze, D. W. Phillion, M. D. Rosen, and J. T. Larsen, Phys. Rev. Lett. **46**, 724 (1981); G. Garban-Labaune, E. Fabre, C. E. Max, R. Fabbro, F. Amiranoff, J. Virmont, M. Weinfeld, and A. Michard, *ibid.* **45**, 1018 (1982).

[5]C. Montes, Phys. Rev. Lett. **50**, 1129 (1983).

[6]R. W. Short and E. A. Williams, Phys. Fluids **26**, 2342 (1983).

[7]T. Speziale, J. F. McGrath, and R. L. Berger, Phys. Fluids **23**, 1275 (1977).

[8]W. L. Kruer, K. G. Estabrook, and K. H. Sinz, Nucl. Fusion **13**, 952 (1973).

[9]J. Gardner and S. Bodner, Phys. Rev. Lett. **47**, 1137 (1981).

[10]R. Giles, R. Fedosejevs, and A. A. Offenberger, Phys. Rev. A **26**, 1113 (1982).

[11]C. L. Tang, J. Appl. Phys. **37**, 2945 (1966).

[12]G. Laval, R. Pellat, D. Pesme, A. Ramani, M. N. Rosenbluth, and E. A. Williams, Phys. Fluids **20**, 2049 (1977).

[13]D. W. Forslund, J. M. Kindel, and E. L. Lindman, Phys. Fluids **18**, 1002 (1975); J. Drake, P. K. Kaw, Y. C. Lee, G. Schmidt, C. S. Liu, and M. N. Rosenbluth, *ibid.* **17**, 778 (1974).

[14]A. A. Offenberger, M. R. Cervenan, A. M. Yam, and A. W. Pasternak, J. Appl. Phys. **47**, 1451 (1976); A. A. Offenberger, A. Ng, and M. R. Cervenan, Can. J. Phys. **56**, 381 (1978); A. Ng, L. Pitt, D. Salzmann, and A. A. Offenberger, Phys. Rev. Lett. **42**, 307 (1979).

[15]C. Montes and J. Peyraud, J. Phys. (Paris), Colloq. **41**, C3-387 (1980); Proc. Soc. Photo-Opt. Instrum. Eng. **228**, 199 (1981).

[16]J. J. Thomson, Nucl. Fusion **15**, 237 (1975).

[17]V. Fuchs, Phys. Fluids **19**, 1554 (1976).

[18]F. Y. F. Chu and C. F. F. Karney, Phys. Fluids **20**, 1728 (1977).

[19]S. J. Karttunen and R. R. E. Salomaa, Plasma Phys. **21**, 247 (1979).

[20]C. Montes, in *Proceedings of the 1982 International Conference on Plasma Physics,* edited by H. Wilhelmsson and J. Weiland (Chalmers University of Technology, Göteborg, 1982), p. 188.

[21]C. E. Max, in *Proceedings of the Les Houches Summer School, Session XXXIV,* edited by R. Balian and J. C. Adam (North-Holland, Amsterdam, 1982), p. 332.

[22]V. N. Tsytovich, *Nonlinear Effects in Plasma* (Plenum, New York, 1970).

[23]D. W. Phillon, W. L. Kruer, and V. C. Rupert, Phys. Rev. Lett. **39**, 1529; W. L. Kruer, Phys. Fluids **23**, 1273 (1980).

[24]C. Montes, Astrophys. J. **216**, 329 (1977); C. Montes, Phys. Rev. A **20**, 1081 (1979); C. Montes, J. Peyraud, and M. Hénon, Phys. Fluids **22**, 176 (1979); C. Montes, *Plasma Physics: Nonlinear Theory and Experiments* (Plenum, New York, 1977), p. 222.

[25]R. H. Stolen and Chinlon Lin, Phys. Rev. A **17**, 1448 (1978).

[26]E. Durand, *Solutions Numériques des Equations Algébriques* (Masson, Paris, 1960), p. 152.